SPACE WEATHER, VOL. 11, 1–9, doi:10.1002/2013SW000990, 2013

Simulation of the 23 July 2012 extreme space weather event: What if this extremely rare CME was Earth directed?

Chigomezyo M. Ngwira,[1,2] Antti Pulkkinen,[2] M. Leila Mays,[1,2]
Maria M. Kuznetsova,[2] A. B. Galvin,[3] Kristin Simunac,[3]
Daniel N. Baker,[4] Xinlin Li,[4] Yihua Zheng,[2] and Alex Glocer[2]

Received 18 September 2013; revised 28 October 2013; accepted 11 November 2013.

[1] Extreme space weather events are known to cause adverse impacts on critical modern day technological infrastructure such as high-voltage electric power transmission grids. On 23 July 2012, NASA's Solar Terrestrial Relations Observatory-Ahead (STEREO-A) spacecraft observed in situ an extremely fast coronal mass ejection (CME) that traveled 0.96 astronomical units (~1 AU) in about 19 h. Here we use the Space Weather Modeling Framework (SWMF) to perform a simulation of this rare CME. We consider STEREO-A in situ observations to represent the upstream L1 solar wind boundary conditions. The goal of this study is to examine what would have happened if this Rare-type CME was Earth-bound. Global SWMF-generated ground geomagnetic field perturbations are used to compute the simulated induced geoelectric field at specific ground-based active INTERMAGNET magnetometer sites. Simulation results show that while modeled global *SYM-H* index, a high-resolution equivalent of the *Dst* index, was comparable to previously observed severe geomagnetic storms such as the Halloween 2003 storm, the 23 July CME would have produced some of the largest geomagnetically induced electric fields, making it very geoeffective. These results have important practical applications for risk management of electrical power grids.

Citation: Ngwira, C. M., A. Pulkkinen, M. Leila Mays, M. M. Kuznetsova, A. B. Galvin, K. Simunac, D. N. Baker, X. Li, Y. Zheng, and A. Glocer (2013), Simulation of the 23 July 2012 extreme space weather event: What if this extremely rare CME was Earth directed?, *Space Weather*, *11*, doi:10.1002/2013SW000990.

1. Introduction

[2] Space weather is a major concern for modern day society because of its adverse impacts on technological infrastructure such as power grids, oil pipelines, and global navigation systems. Earth directed space weather events such as coronal mass ejections (CMEs) are the main drivers of the most extreme geomagnetic storms in the near-Earth space environment. The threat of adverse impacts on critical technological infrastructure like power grids has prompted renewed interest in extreme geomagnetic storms in order to further our understanding of these events [see, e.g., *Thomson et al.*, 2011; *Pulkkinen et al.*, 2012; *Ngwira et al.*, 2013, and references therein].

[3] Historically, the coupling of fast moving CMEs to planetary magnetospheres through the solar wind has been a subject of intense study [e.g., *Baker et al.*, 1996; *Gombosi et al.*, 2000; *Palmroth et al.*, 2004; *Pulkkinen et al.*, 2010; *Guo et al.*, 2012, and references therein]. First principles physics-based three-dimensional (3-D) global magnetohydrodynamics (MHD) models play a critical role in simulating the large-scale dynamics of magnetospheric systems and represent a very important component of attempts to understand the response of the magnetosphere-ionosphere system to varying solar wind conditions [e.g., *Groth et al.*, 2000; *Gombosi et al.*, 2000]. Upstream L1 solar wind observations are normally used as driving conditions for many global simulation models of the large-scale magnetosphere-ionosphere system.

Additional supporting information may be found in the online version of this article.

[1]Department of Physics, Catholic University of America, Washington, District of Columbia, USA.
[2]NASA Goddard Space Flight Center, Space Weather Laboratory, Greenbelt, Maryland, USA.
[3]Institute for the Study of Earth, Oceans, and Space, University of New Hampshire, Durham, New Hampshire, USA.
[4]Laboratory for Atmospheric and Space Physics, University of Colorado Boulder, Boulder, Colorado, USA.

Corresponding author: C. M. Ngwira, NASA Goddard Space Flight Center, Code 674, The Catholic University of America, Building 21 Room 159, Greenbelt, MD 20771, USA. (chigongwira@yahoo.co.uk)

1542-7390/13/10.1002/2013SW000990

[4] Understanding of the magnetosphere and ionosphere dynamics during extreme solar wind driving is still a major challenge mainly because of a lack of data during time intervals when the magnetosphere is being strongly driven [see, e.g., *Ridley et al.*, 2006]. Therefore, complete or good quality solar wind measurements from observed extreme space weather events can provide vital information for the study on the Earth's response to extreme space weather, particularly in relation to geomagnetically induced currents (GIC) that are a threat to the safe and efficient operation of high-voltage electrical power transmission systems.

[5] On 23 July 2012, a CME was hurled away from the Sun's active region AR1520 with a Rare speed (R-type) of approximately 2500 $\pm$ 500 km/s [*Baker et al.*, 2013]. The R-type CME typification is based on a recent report by *Evans et al.* [2013]. This particular CME was not Earth directed, but was the fastest ever observed in situ by NASA's STEREO-A (Solar Terrestrial Relations Observatory-Ahead of Earth in its orbit) spacecraft [*Kaiser et al.*, 2008]. A detailed account of the interplanetary properties of this CME is given by *Russell et al.* [2013]. Also, this unusual space weather phenomenon produced the highest flux ever recorded by STEREO-A with a solar energetic particle (up to 100 MeV) event estimate of $\sim 4.52 \times 10^4$ pfu, where pfu = proton flux unit = particles/sr cm^2 s. Events such as the 23 July 2012 CME event offer an unprecedented opportunity to explore the effects of extreme space weather.

[6] For the purpose of the present study, we consider NASA's STEREO-A spacecraft in situ observations to represent the upstream L1 solar wind boundary conditions that are used as driving conditions for the global magnetospheric MHD model. Our primary goal is to examine the geomagnetically induced electric field response that this R-type space weather event could have generated had it hit the Earth.

2. MHD Modeling Process

[7] In this paper, the modeling process is performed using the Space Weather Modeling Framework (SWMF) developed at the University of Michigan [*Tóth et al.*, 2005]. The MHD simulations were performed using the facilities available at the Community Coordinated Modeling Center (CCMC) operating at NASA Goddard Space Flight Center. SWMF is a flexible framework that integrates various physics-based numerical models into a high-performance coupled model via a standardized interface and a highly efficient parallel coupling toolkit. The SWMF creates an environment where simulations that were impossible with individual physics models can be performed. The core design and implementation of the SWMF is described in-depth by *Tóth et al.* [2005].

[8] In the MHD model, the ground magnetic perturbations are computed by integrating over all the magnetospheric, ionospheric, and gap region current systems within the near-Earth space environment using Biot-Savart [see, e.g., *Yu et al.*, 2010]. Also, the modeled *Dst* index is calculated by solving the Biot-Savart integral for all the electric currents within the global magnetospheric simulation domain from the inner boundary outward and taking the magnetic field disturbance along the z axis at the center of the coordinate system. In the present simulation, the ring current energy injection is estimated using the planetary *SYM-H* index, which is essentially a high-resolution (1 min) model equivalent of the *Dst* index. The ring current dynamics are simulated in a realistic fashion using the Rice Convection Model (RCM) coupled to BATS-R-US [*De Zeeuw et al.*, 2004].

[9] The SWMF simulation performance is well calibrated from previously observed events, and a number of validation works have been widely reported [see, e.g., *Yu and Ridley*, 2008; *Pulkkinen et al.*, 2009; *Yu et al.*, 2010]. For instance, *Pulkkinen et al.* [2009] showed that the model results can be slightly overestimated but were generally comparable to the ground magnetometer observations. In addition, *Yu et al.* [2010] reveals that SWMF generated ground perturbations can be more accurately modeled by inclusion of magnetospheric driven current systems within the near-Earth space environment. This is all in agreement with work by *Pulkkinen et al.* [2011] which demonstrates that increasing the global SWMF spatial resolution and the inclusion of the ring current dynamics is seen to improve the SWMF capability to generate more realistic ground magnetic field fluctuations. Therefore, all these works discussed above demonstrate that the SWMF modeling is reliable and sufficient for our applications.

[10] The SWMF predicts in a self-consistent manner the dynamic response of the large-scale magnetosphere to changing solar wind conditions using the block-adaptive tree solar wind Roe-type upwind scheme (BATS-R-US) global MHD code [*Powell et al.*, 1999]. Here the global magnetosphere cavity is simulated in a moving computational box defined by dimensions –224 $R_E < x <$ 32 R_E, –128 $R_E <$ $y <$ 128 R_E, –128 $R_E < z <$ 128 R_E, where R_E is the Earth radius, with the Earth placed at the center. The dipole tilt in the simulation is set to update throughout each run so that it is dependent on the day of the year and the time of the day. The simulation was carried out on a block-adaptive grid having a sparse resolution of 1/4R_E, resulting in about 1 million global MHD model cells. We set interplanetary magnetic field (IMF) $\mathbf{B}x = 0$ for this simulation to keep divergence-free condition. Generally, SWMF simulations at CCMC suggest that the results are not very sensitive to $\mathbf{B}x$, but to some extent, this condition may lead to a slight modification in the progression of events, as there is no magnetic rotation along the x axis [see, e.g., *Groth et al.*, 2000]. However, this condition does not have a significant bearing for our applications because the geomagnetic strength is largely controlled by $\mathbf{B}z$ component. Furthermore, magnetopause currents are mapped at 3 R_E, while the inner magnetosphere boundary is set at 2.5 R_E. It should be noted that inner magnetosphere currents also map into the ionosphere.

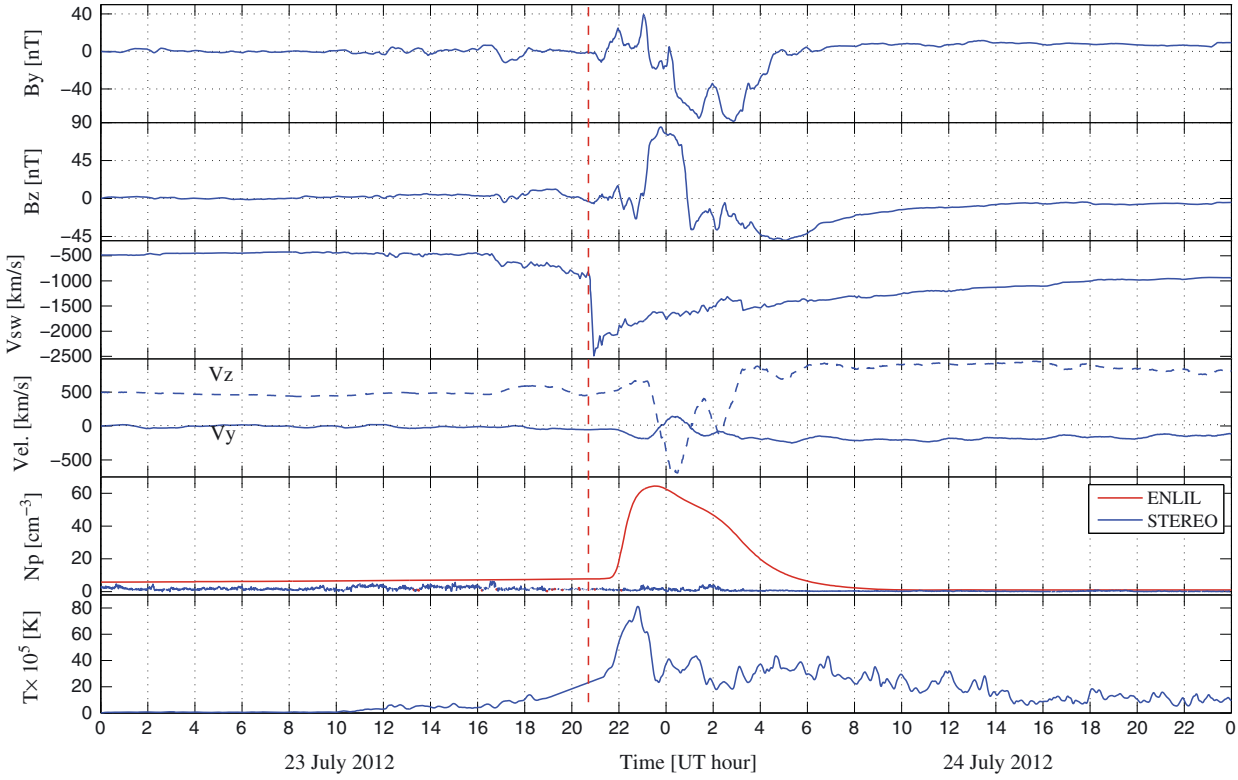

Figure 1. Solar wind in situ observations from the STEREO-A spacecraft. From top to bottom are: the IMF **B*y***, IMF **B*z***, plasma bulk speed (*Vsw*), the velocity *Vy* (solid) and *Vz* (dashed) components, the solar wind density (*Np*), and the temperature (Temp). Note that the density (red trace) is derived using the WSA-ENLIL 3-D MHD heliosphere model due to challenges in extracting the PLASTIC density data.

[11] The BATS-R-US inner boundary couples to an ionosphere model represented by a height-integrated potential solver [*De Zeeuw et al.*, 2004; *Ridley et al.*, 2004]. The low-latitude boundary of the ionosphere based on the mapping from the MHD inner boundary is imposed at 10° latitude. A fixed density of 28/cm^3 is used at the inner boundary with the temperature (or pressure) and magnetic field allowed to vary to the given solution. The auroral conductance (realistic oval) is driven by a solar EUV component with a solar flux F10.7 of 99.8 and field-aligned electric currents. The dayside processes and structure of the thermosphere and ionosphere are determined by solar illumination, while the nightside "starlight" and polar cap Pedersen conductance are assumed to be 1 mho and 0.25 mho, respectively. The high-latitude particle precipitation in the MHD code is fully dependent upon the local field-aligned currents (FACs), which forms a coarse auroral oval structure, although there is little conductance near midnight due to the weak FAC [*Ridley et al.*, 2004].

3. Data Sources and Methods

[12] NASA's STEREO mission is comprised of two twin spacecraft in heliospheric orbit, with one spacecraft trailing the Earth (behind) and the other leading (ahead), with the objective of understanding CME initiation and propagation. Unprecedented CME observations can be made using a combination of STEREO/SECCHI (Sun Earth Connection Coronal and Heliospheric Investigation) coronagraph [*Howard et al.*, 2008], and L1 Lagrange point coronagraphs such as the SOHO/LASCO, SOlar and Heliospheric Observatory/Large Angle Spectroscopic Coronagraph, respectively [*Domingo et al.*, 1995; *Brueckner et al.*, 1995], thereby furthering our understanding of how space weather affects the entire solar system.

[13] On 23 July 2012 the STEREO spacecraft had a separation of 123.88°, and the STEREO-A spacecraft had a heliographic longitude of 121.26° and latitude of 1.74°. The CME became visible in SOHO/LASCO C2 at 02:36 UT and was detected in situ at STEREO-A at 20:55 UT [*Russell et al.*, 2013]. *Baker et al.* [2013] determined the three-dimensional CME parameters to be 2500 ± 500 km/s with a direction of $125^{\circ}{}^{+15^{\circ}}_{-5^{\circ}}$ longitude, 2 ± 10° latitude (HEEQ coordinates), and a full width of 140° ± 30°. Additionally, the CME parameters were derived by the NASA Goddard Space Weather Research Center at the CCMC in near-real time (with only STEREO-A and SOHO images available) to give a CME speed of 3435 km/s in the direction of

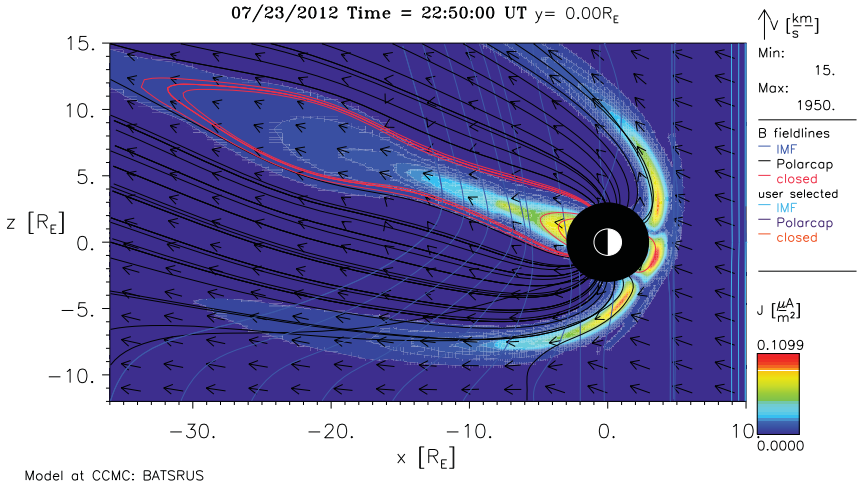

Figure 2. Example simulated cross section of the magnetosphere at 22:50 UT on 23 July 2012. The plot shows the current density, *J*, in color; solar wind velocity, *Vx*, arrows; and magnetic field, **B***x*, field line traces. The IMF and magnetic field line traces can be system defined (**B** field lines) or user selected.

144° longitude, –15° latitude, and a full width of 160° [*Baker et al.*, 2013].

[14] In situ solar wind plasma and magnetic field data are measured respectively by the PLASTIC (Plasma and Suprathermal Ion Composition) and IMPACT (In situ Measurements of Particles And CME Transients) investigations on board the STEREO spacecraft [*Galvin et al.*, 2008; *Acuña et al.*, 2008]. Figure 1 exhibits the solar wind upstream boundary conditions that were used as input to the SWMF model. STEREO-A observations from the IMPACT (level 2) and PLASTIC instruments are shown. The figure displays from top to bottom: the IMF **B***y* component, IMF **B***z* component, plasma bulk speed, *Vsw*, which is used as velocity *Vx* input, the velocity *Vy* (solid), and *Vz* (dashed) components, and the solar wind density (*Np*), i.e., blue trace for STEREO-A observations and red for WSA-ENLIL 3-D MHD numerical heliospheric model [see, e.g., *Arge and Pizzo*, 2000; *Odstrcil et al.*, 2004]. The temperature (Temp) is shown in the bottom panel.

[15] WSA-ENLIL is a time-dependent 3-D MHD heliosphere model used to study temporal and spatial evolution of large-scale space weather events [see, e.g., *Arge et al.*, 2004; *Taktakishvili et al.*, 2009, and references therein]. WSA (Wang-Sheeley-Arge) models the global magnetic field between the Sun and the bounding spherical surface and considers the magnetic field to be radial [*Arge and Pizzo*, 2000]. These data are the basis for the ENLIL model [*Odstrcil et al.*, 2004]. ENLIL also accepts inputs from the cone model [*Xie et al.*, 2004], which provides the halo CME parameters and the propagation through the interplanetary space, determined using coronagraph images. Note that as a first-order approximation, the density data from the real-time WSA-ENLIL cone model simulation carried out at the STEREO-A location by the SWRC forecasting staff is used in the present case. This is due to ongoing challenges in extracting good PLASTIC density data, as the PLASTIC instrumentation can suffer from saturation effects during very severe storm conditions, thereby limiting the accurate determination of solar wind parameters [*Galvin et al.*, 2008]. It should be mentioned that the WSA-ENLIL MHD model can sometimes overestimate the density, therefore, this data is only used for analysis of the worst case scenario had this CME been Earth directed.

[16] Also, the observations in Figure 1 show strong negative **B***z* with a peak of ∼−49 nT and an even larger northward amplitude of ∼84 nT. This CME traveled nearly 1 AU in about 19 h (if we consider the eruption time of ∼02:05 as seen in EUVI images) with a maximum observed in situ bulk speed of 2300 ± 100 km/s, as estimated from the most recent calibration performed by the PLASTIC team at the time of this writing. Generally, this CME had large velocity *Vz* values that can affect the orientation of the magnetotail and possibly some of the dynamics, which in turn can enhance the asymmetry in the North and South polar cap. On the other hand, the temperature values are consistent with other severe CMEs such as the October 2003 Halloween storm.

[17] From the SWMF-generated magnetic perturbations, using the solar wind inputs described above, we determined the geoelectric fields using the plane wave method [see, e.g., *Cagniard*, 1953; *Pirjola*, 1982]. The model generates magnetic field perturbations at locations of active INTERMAGNET (`www.intermagnet.org`) magnetometer sites. The geoelectric field components $E_{x,y}$ can be computed in terms of the perpendicular geomagnetic field components $B_{y,x}$ as

$$E_{x,y} = \pm \frac{1}{\sqrt{\pi\,\mu_0\,\sigma}} \int_{-\infty}^{t} \frac{1}{\sqrt{t-u}} \frac{\mathrm{d}B_{y,x}(u)}{\mathrm{d}t}\,\mathrm{d}u \qquad (1)$$

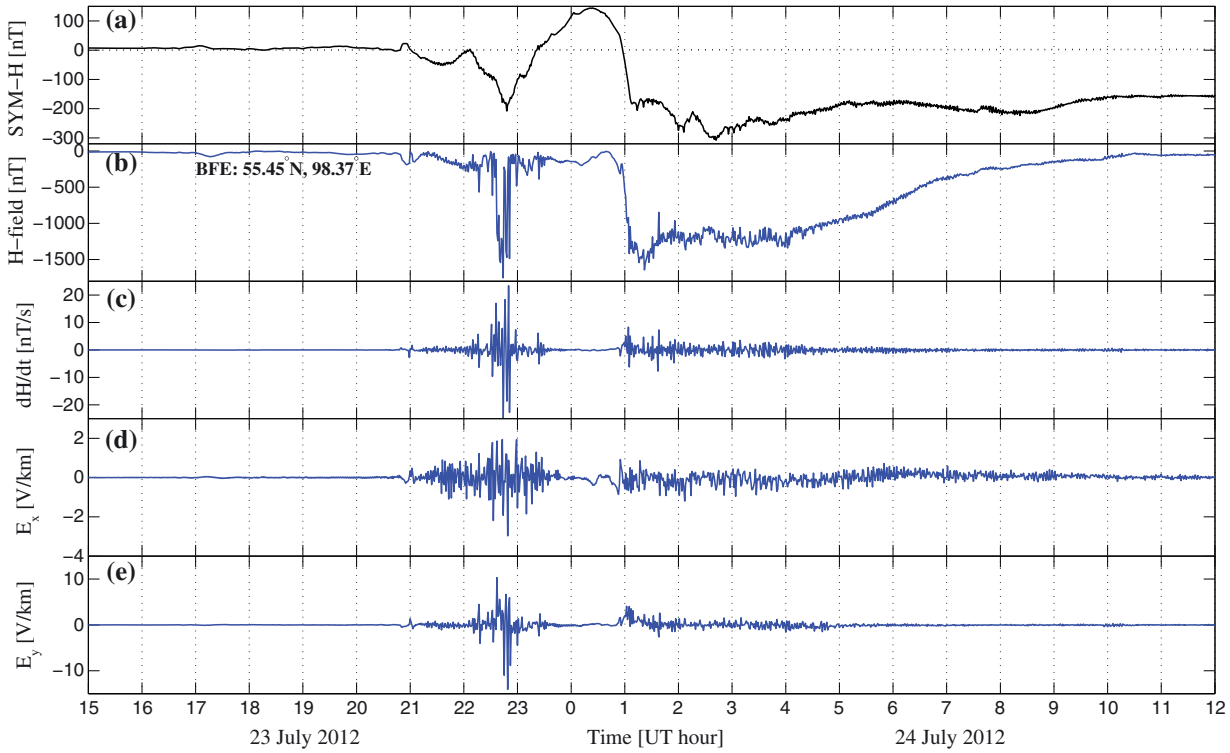

Figure 3. The SWMF-derived global *SYM-H* index and an example of the model ground magnetic perturbations and the calculated geoelectric field response at the Brorfelde high-latitude ground magnetometer site. The Brorfelde station had the largest geoelectric fields for this simulation.

where μ_0 is the permeability of free space and σ is the effective conductivity. The resistive-end Quebec ground conductivity model was applied [see *Pulkkinen et al.*, 2012], since our interest is in extreme event cases. Strictly speaking, the plane wave method is not directly applicable here, because the method assumes that the magnetic field signal includes both external and internal contributions. However, this will not introduce significant errors in the modeled geoelectric fields as the internal contribution is relatively small compared to the external.

4. Simulation Results and Discussions

[18] Illustrated in Figure 2 is a cross section of the magnetosphere's response to the simulated CME in the $Y = 0$ plane at 22:50 UT on 23 July 2012. The figure shows an enhanced current density, J, with stretched closed field lines (red). This period roughly corresponds to the time of the first *SYM-H* index minimum, as exhibited in Figure 3. Figure 3 shows the SWMF-derived global *SYM-H* index, and an example of the modeled geomagnetic perturbations and the calculated ground-induced geoelectric field (E_x and E_y, respectively) response at the Danish Brorfelde (BFE: 55.45°N, 98.37°E, geomagnetic) high-latitude magnetometer site. The results reveal that the *SYM-H* response pattern had two negative excursions, with the first excursion on 23 July reaching a minimum of –201 nT at about 22:50 UT followed by a quick recovery period, while the second excursion on 24 July started after 00:45 before reaching a minimum of about –300 nT around 02:42 UT and was followed by a long recovery period. This long recovery phase can be related to the IMF **B***z* component which remained southward for a long time as revealed in Figure 1. Evidently, the two main phases are separated by a strong positive *SYM-H* (150 nT) response, which is associated to the reversal of the IMF **B***z* component from southward to northward orientation with a maximum of ∼84 nT near 23:49 UT on 23 July.

[19] On the basis of the *SYM-H* index amplitudes, this storm could be classified as a "common" severe event in comparison with the strength of previously observed events, e.g., the 31 March 2001 or the Halloween 29 October 2003 storms with minimum *SYM-H* values around –387 nT and –383 nT, respectively. However, the computed maximum induced geoelectric fields for the present event are slightly larger, as will be demonstrated below. It should be mentioned here that a recent investigation of the 23 July CME using an empirical *Dst* model suggests that the *Dst* response could have been considerably stronger (above 500 nT) under optimal coupling conditions [see *Baker et al.*, 2013].

[20] Figure 4 depicts the maximum induced geoelectric fields at all the individual ground sites used in this study. The figure shows two simulation results, i.e.,

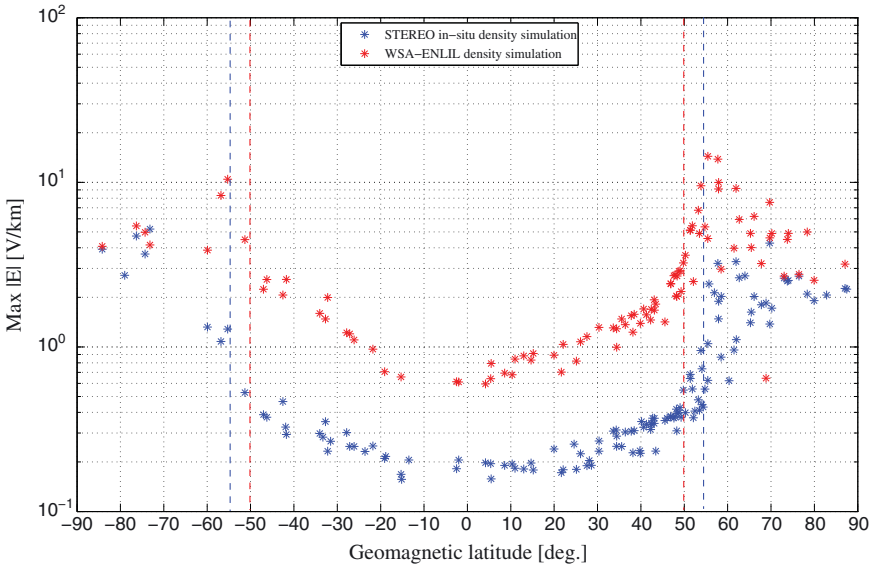

Figure 4. The maximum-induced ground electric field (blue) simulated using STEREO in situ density and (red) simulated using WSA-ENLIL model density. Note that the time of the maximum field varies from site to site. The red and blue dashed lines show the locations of the transition regions between middle and high latitudes, which are related to the auroral electrojet current system and is described in-depth by *Pulkkinen et al.* [2012] and more recently by *Ngwira et al.* [2013].

geoelectric field simulated using STEREO in situ real-time density (blue) and the other using WSA-ENLIL model density (red). As mentioned earlier, our interest is in a worst case scenario, therefore, we only discuss results simulated using the WSA-ENLIL density. Here the latitude threshold boundary (red dashed line) is located around 50° MLAT and is consistent with observations for severe geomagnetic storms [e.g., *Thomson et al.*, 2011; *Pulkkinen et al.*, 2012; *Ngwira et al.*, 2013]. The location of these transition regions between middle and high latitudes is related to the dynamics (strengthening and widening) of the auroral current system [*Ngwira et al.*, 2013]. For a higher density, this region can be shifted to much lower latitudes due to enhancement and expansion of the auroral current that can be linked to stronger region-2 Birkeland currents [e.g., *De Zeeuw et al.*, 2004], as more solar wind plasma becomes available in the magnetosphere. Additionally, we believe that the auroral current system expansion could also be driven by the compression of the magnetosphere as the pressure front hits the magnetopause boundary, leading to an increase of the dayside magnetic field and the Chapman-Ferraro current [*Zesta et al.*, 2013].

[21] We also note that the geoelectric fields calculated for midlatitude stations in this study are significantly higher (two to five times) compared to values reported by *Pulkkinen et al.* [2012] and *Ngwira et al.* [2013] for observed extreme geomagnetic storm events. For instance, the peak geoelectric field at Hermanus Observatory (HER: 42.3°S, 84.4°E, geomagnetic) is ∼1.50 V/km for the present case and about ∼0.29 V/km from results reported by *Ngwira et al.* [2013]. Furthermore, the current version of the MHD model includes the ring current dynamics; however, it does not include the equatorial electrojet (EEJ) and solar quiet (Sq) current systems, which could explain the small values of the geoelectric field around the dip equator and low-latitude regions. *Ngwira et al.* [2013] showed that during selected geomagnetic storms, ground-induced geoelectric fields can be enhanced on the dayside dip equator due to intensification of the EEJ current system, which is in turn driven by the cowling conductivity effect.

[22] Lastly, the present results show that the largest simulated induced geoelectric fields were observed on the nightside in the European high-latitude sector. One of the interesting features of the result in Figure 4 is the value of the maximum ground-induced geoelectric field with a peak value of 14.38 ± 2.86 V/km occurring at the Brorfelde magnetometer station [see Figures 3d and 3e]. This value is 3 V/km higher than the value determined for previously observed events during the period 1989 to 2005 (0.2 to 11.4 V/km), as reported in a recent study by *Ngwira et al.* [2013]. From that study, the maximum-induced geoelectric field value of about 11.4 V/km was reported to have occurred during the Halloween 2003 storm, whereas two cases presented in the present study have maximum geoelectric field values above 13.5 V/km. These large geoelectric fields are associated with the auroral current system, which is in turn driven by substorm-related activity, as further discussed below. Figure 5 demonstrates that there are sharp changes in the magnetotail magnetic field components X and Z at about 22:48 UT, as marked by the vertical

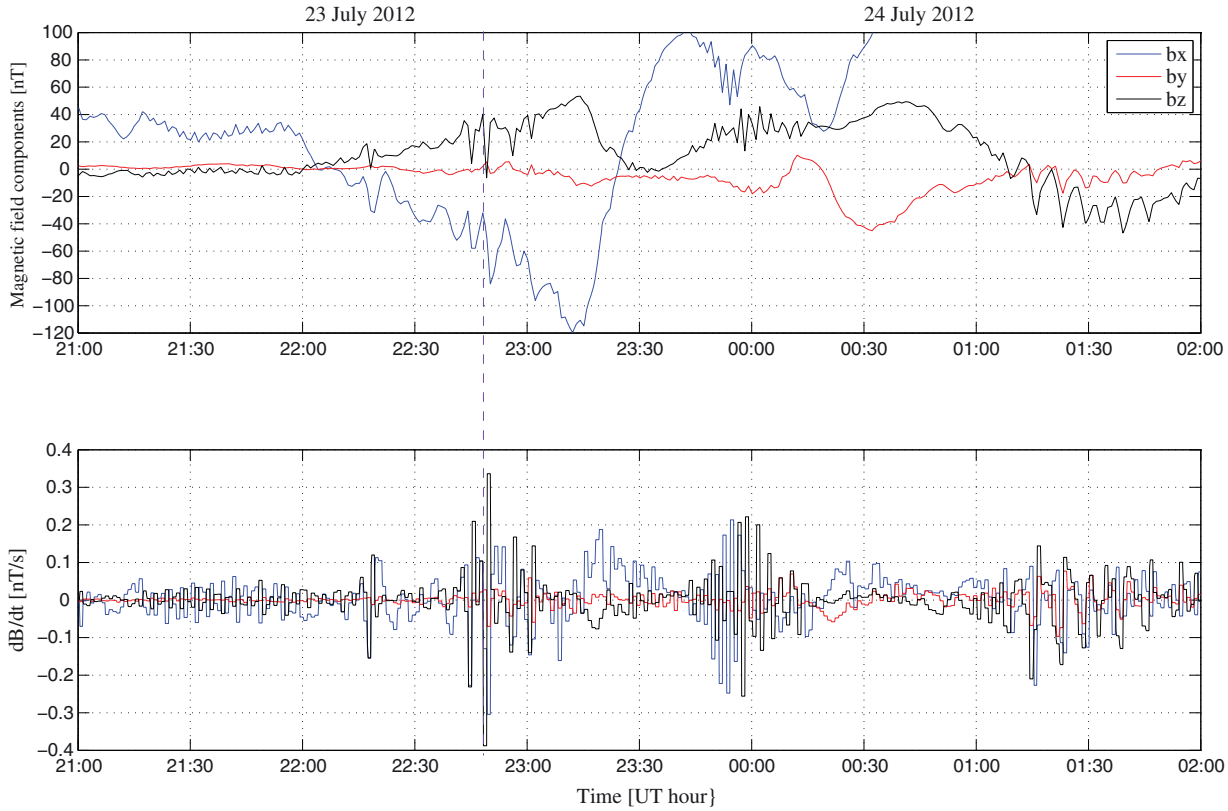

Figure 5. Plot showing the (top) geomagnetic field components and (bottom) their respective rate-of-change for a selected location (X = –12 R_E, Y = 0 and Z = 4 R_E) in the magnetotail.

purple line. This is roughly the same time that a plasmoid feature (see supporting information) is released in the tail region. The corresponding rate-of-change components show rapid variations at the same instance.

[23] Plasmoids, which are associated with substorm onset, are large magnetic structures that are formed by separating closed plasma sheet field lines in the near-Earth magnetotail through magnetic reconnection [e.g., *Moldwin and Hughes*, 1993; *Baker et al.*, 1996]. As the plasmoid grows, a magnetic neutral point forms in the near-Earth region, then the plasmoid is pushed tailward at high speeds, and some amount of plasma is accelerated toward the Earth, causing intensification of the auroral current at Earth's high-latitude nightside and accompanying geomagnetic disturbance [e.g., *Baker et al.*, 1996]. As demonstrated in Figure 5, the most noteworthy changes in the magnetotail region during the disturbed period can be related to the large changes in the geoelectric field on the ground at about 22:50 UT. This further reinforces our assertion that the largest geoelectric fields are related to substorm activity.

5. Conclusion

[24] In this paper, we considered STEREO-A in situ observations to represent the upstream L1 solar wind boundary conditions that were used as driving conditions for the global MHD model. Our results show that the largest simulated induced geoelectric fields were observed on the nightside in the European high-latitude sector. Further investigation reveals that this is related to magnetospheric substorm activity, as simulated plasmoid features were observed in the magnetotail around this same time period (22:50 UT).

[25] Generally, higher levels of geoelectric fields can drive large GIC in Earth conductors such as power grids, and therefore are a source of concern for power grid operators [e.g., *Pulkkinen et al.*, 2005, and references therein]. Consequently, had the 23 July CME hit Earth, there is a possibility that it could have produced comparable or slightly larger geomagnetically induced electric fields to those produced by previously observed Earth directed events such as the March 1989 storm or the Halloween 2003 storms. The implication is that, power systems could have been exposed to high levels of electric currents with the potential to drive large amplitude GIC, thereby increasing their susceptibility to GIC risks. It is important to emphasize here that a power system's response to geomagnetic disturbances is governed by several factors, and the geoelectric field amplitude is only one part of the full power system impact analysis [*North America Electric Reliability Corporation (NERC)*, 2012]. Lastly, we would like to

point out that much more detailed investigations of the 23 July CME are still ongoing, including the effects of changing the CME magnetic field structure orientation seen by the magnetosphere that may amplify the storm strength from that presented here.

[26] **Acknowledgments.** Authors acknowledge Mei-Ching Fok and Ja Soon Shim for useful discussions. All SWMF/WSA-ENLIL simulations were performed through the runs-on-request system at the CCMC located at NASA Goddard Space Flight Center. The SMWF/BATS-R-US Model was developed at the University of Michigan. SOHO is a mission of international cooperation between the European Space Agency and NASA. C.M. Ngwira is supported by EPRI under contract EPRI-18403, while A.B. Galvin and K. Simunac are supported by NASA grant NAS5-00132. The authors also thank their EURISGIC partners (European Risk from Geomagnetically Induced Currents), an EU/FP7 Space Research project, for useful discussions on this work.

References

Acuña, M. H., D. Curtis, J. L. Scheifele, C. T. Russell, P. Schroeder, A. Szabo, and J. G. Luhmann (2008), The STEREO/IMPACT magnetic field experiment, *Space Sci. Rev.*, *136*, 203–226, doi:10.1007/s11214-007-9259-2.

Arge, C. N., and V. J. Pizzo (2000), Improvement in the prediction of solar wind conditions using near-real time solar magnetic field updates, *J. Geophys. Res.*, *105*, 10,465–10,480, doi:10.1029/1999JA000262.

Arge, C. N., J. G. Luhmann, D. Odstrcil, C. J. Schrijver, and Y. Li (2004), Stream structure and coronal sources of the solar wind during the May 12th, 1997 CME, *J. Atmos. Sol. Terr. Phys.*, *66*, 1295–1309.

Baker, D. N., T. I. Pulkkinen, V. Angelopoulos, W. Baumjohann, and R. L. McPherrron (1996), Neutral line model of substorm: Past results and present view, *J. Geophys. Res.*, *101*(A6), 12,975–13,010, doi:10.1029/95JA03753.

Baker, D. N., X. Li, A. Pulkkinen, C. M. Ngwira, M. L. Mays, A. B. Galvin, and K. D. C. Simunac (2013), A major solar eruptive event in July 2012: Defining extreme space weather scenarios, *Space Weather*, *11*, 1–7, doi:10.1002/swe.20097.

Brueckner, G. E., et al. (1995), The large angle spectroscopic coronagraph, *Sol. Phys.*, *162*, 357–402.

Cagniard, L. (1953), Basic theory of the magneto-telluric methods of geophysical prospecting, *Geophysics*, *18*(3), 605–635.

De Zeeuw, D. L., S. Sazykin, R. A. Wolf, T. I. Gombosi, A. J. Ridley, and G. Tóth (2004), Coupling of a global MHD code and an inner magnetosphere model: Initial results, *J. Geophys. Res.*, *109*, A12219, doi:10.1029/2003JA010366.

Domingo, V., B. Fleck, and A. I. Poland (1995), The SOHO mission, *Sol. Phys.*, *162*, 1–37.

Evans, R. M., A. A. Pulkkinen, Y. Zheng, M. L. Mays, A. Taktakishvili, M. M. Kuznetsova, and M. Hesse (2013), The SCORE scale: A coronal mass ejection typification system based on speed, *Space Weather*, *11*, 333–334, doi:10.1002/swe.20058.

Galvin, A. B., et al. (2008), The Plasma and Suprathermal Ion Composition (PLASTIC) investigation on the STEREO observatories, *Space Sci. Rev.*, *136*, 437–486, doi:10.1007/s11214-007-9296-x.

Gombosi, T. I., D. L. De Zeeuw, C. P. T. Groth, K. G. Powell, and Q. F. Stout (2000), Multiscale MHD simulation of a coronal mass ejection and its interaction with the magnetosphere-ionosphere system, *J. Atmos. Sol. Terr. Phys.*, *62*, 1515–1525.

Groth, C. P. T., D. L. De Zeeuw, T. I. Gombosi, and K. G. Powell (2000), Global three-dimensional MHD simulation of a space weather event: CME formation, interplanetary propagation, and interaction with the magnetosphere, *J. Geophys. Res.*, *105*(A11), 25,053–25,078.

Guo, J., X. Feng, B. A. Emery, and Y. Wang (2012), Efficiency of solar wind energy coupling to the ionosphere, *J. Geophys. Res.*, *117*, A07303, doi:10.1029/2012JA017627.

Howard, R. A., et al. (2008), Sun Earth Connection Coronal and Heliospheric Investigation (SECCHI), *Space Sci. Rev.*, *136*, 67–115, doi:10.1007/s11214-008-9341-4.

Kaiser, M. L., T. A. Kucera, J. M. Davila, O. C. St. Cyr, M. Guhathakurta, and E. Christian (2008), The STEREO mission: An introduction, *Space Sci. Rev.*, *136*, 5–16, doi:10.1007/s11214-007-9277-0.

Moldwin, M. B., and W. J. Hughes (1993), Geomagnetic substorm association of plasmoids, *J. Geophys. Res.*, *98*, 81–88.

Ngwira, C. M., A. Pulkkinen, F. D. Wilder, and G. Crowley (2013), Extended study of extreme geoelectric field event scenarios for geomagnetically induced current applications, *Space Weather*, *11*, 121–131, doi:10.1002/swe.20021.

North America Electric Reliability Corporation (NERC) (2012), Special reliability assessment interim report: Effects of geomagnetic disturbances on bulk power systems, NERC Interim GMD Report, available at `http://www.nerc.com/files/2012GMD.pdf`.

Odstrcil, D., P. Riley, and X. P. Zhao (2004), Numerical simulation of the 12 May 1997 interplanetary CME event, *J. Geophys. Res.*, *109*, A02116, doi:10.1029/2003JA010135.

Palmroth, M., P. Janhunen, T. I. Pulkkinen, and H. E. J. Koskinen (2004), Ionospheric energy input as a function of solar wind parameters: Global MHD simulation results, *Ann. Geophys.*, *22*, 549–566.

Pirjola, R. (1982), Electromagnetic induction in the Earth by a plane wave or by fields of line currents harmonic in time and space, *Geophysica*, *18*(1-2), 1–161.

Powell, K. G., P. L. Roe, T. J. Linde, T. I. Gombosi, and D. L. De Zeeuw (1999), A solution-adaptive upwind scheme for ideal magnetohydrodynamics, *J. Comput. Phys.*, *154* (2), 284–309, doi:10.1006/jcph.1999.6299.

Pulkkinen, A., S. Lindahl, A. Viljanen, and R. Pirjola (2005), Geomagnetic storm of 29–31 October: Geomagnetically induced currents and their relation to problems in the Swedish high-voltage power transmission system, *Space Weather*, *3*, S08C03, doi:10.1029/2004SW000123.

Pulkkinen, A., M. Hesse, S. Habib, L. Van der Zel, B. Damsky, F. Policelli, D. Fugate, W. Jacobs, and E. Creamer (2009), Solar shield: Forecastng and mitigating space weather effects on high-voltage power transmission systems, *Nat. Hazards*, *53*, 333–345, doi:10.1007/s11069-009-9432-x.

Pulkkinen, A., E. Bernabeu, J. Eichner, C. Beggan, and A. W. P. Thomson (2012), Generation of 100-year geomagnetically induced current scenarios, *Space Weather*, *10*, S04003, doi:10.1029/2011SW000750.

Pulkkinen, A., et al. (2011), Geospace environment modeling 2008–2009 challenge: Ground magnetic field perturbations, *Space Weather*, *9*, S02004, doi:10.1029/2010SW000600.

Pulkkinen, T. I., M. Palmroth, P. Janhunen, H. E. J. Koskinen, D. J. McComas, and C. W. Smith (2010), Timing of changes in the solar wind energy input in relation to ionospheric response, *J. Geophys. Res.*, *115*, A00109, doi:10.1029/2010JA015764.

Ridley, A. J., T. I. Gombosi, and D. L. De Zeeuw (2004), Ionospheric control of the magnetosphere: Conductance, *Ann. Geophys.*, *22*, 567–584.

Ridley, A. J., D. L. De Zeeuw, W. B. Manchester, and K. C. Hansen (2006), The magnetospheric and ionospheric response to a very strong interplanetary shock and coronal mass ejection, *Adv. Space Res.*, *38*, 263–272.

Russell, C. T., et al. (2013), The very unusual interplanetary coronal mass ejection of 2012 July 23: A blast wave mediated by solar energetic particles, *Astrophys. J.*, *770*, 38, doi:10.1088/0004-637X/770/1/38.

Taktakishvili, A., M. Kuznetsova, P. MacNeice, M. Hesse, L. Rastàtter, A. Pulkkinen, A. Chulaki, and D. Odstrcil (2009), Validation of the coronal mass ejection predictions at the Earth orbit estimated by ENLIL heliosphere cone model, *Space Weather*, *7*, S03004, doi:10.1029/2008SW000448.

Thomson, A. W. P., E. B. Dawson, and S. J. Reay (2011), Quantifying extreme behavior in geomagnetic activity, *Space Weather*, *9*, S10001, doi:10.1029/2011SW000696.

Tòth, G., et al. (2005), Space weather modeling framework: A new tool for the space science community, *J. Geophys. Res.*, *110*, A12226, doi:10.1029/2005JA011126.

Xie, H., L. Ofman, and G. Lawrence (2004), Cone model for halo CMEs: Application to space weather forecasting, *J. Geophys. Res.*, *109*, A03109, doi:10.1029/2003JA010226.

Yu, Y., and A. J. Ridley (2008), Validation of the space weather modeling framework using ground-based magnetometers, *Space Weather*, *6*, S05002, doi:10.1029/2007SW000345.

Yu, Y., A. J. Ridley, D. T. Welling, and G. Tóth (2010), Including gap region field aligned currents and magnetospheric currents in the MHD calculation of ground-based magnetic field perturbations, *J. Geophys. Res.*, *115*, A08207, doi:10.1029/2009JA014869.

Zesta, E., H. J. Singer, D. Lummerzheim, C. T. Russell, L. R. Lyons, and M. J. Brittnacher (2013), The effect of the January 10, 1997, pressure pulse on the magnetosphere-ionosphere current system, in *Magnetospheric Current Systems*, edited by S.-I. Ohtani et al., pp. 217–226, AGU, Washington D. C., doi:10.1029/GM118p0217.